# Stability of untransformed ferrite in 10Cr ODS steel

Anthony Durand, Denis Sornin, Olivier Taché, Thomas Guilbert, François
Brisset, Ludovic Delbes, Benoît Baptiste, Thierry Baudin, Roland Logé

# Journal Pre-proof

## Stability of untransformed ferrite in 10Cr ODS steel

Anthony DURAND , Denis SORNIN , Olivier TACHÉ ,
Thomas GUILBERT , François BRISSET , Ludovic DELBES ,
Benoît BAPTISTE , Thierry BAUDIN , Roland LOGÉ
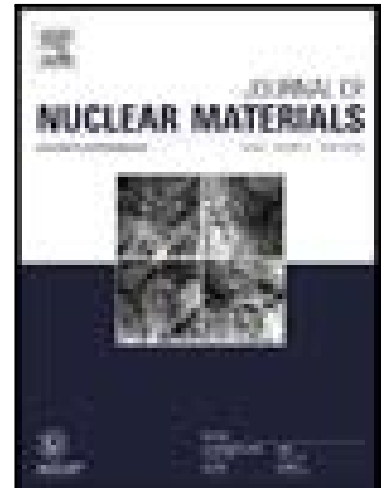
Please cite this article as: Anthony DURAND , Denis SORNIN , Olivier TACHÉ , Thomas GUILBERT , François BRISSET , Ludovic DELBES , Benoît BAPTISTE , Thierry BAUDIN , Roland LOGÉ , Stability of untransformed ferrite in 10Cr ODS steel, *Journal of Nuclear Materials* (2022), doi: https://doi.org/10.1016/j.jnucmat.2022.154146

This is a PDF file of an article that has undergone enhancements after acceptance, such as the addition of a cover page and metadata, and formatting for readability, but it is not yet the definitive version of record. This version will undergo additional copyediting, typesetting and review before it is published in its final form, but we are providing this version to give early visibility of the article. Please note that, during the production process, errors may be discovered which could affect the content, and all legal disclaimers that apply to the journal pertain.

# Stability of untransformed ferrite in 10Cr ODS steel

Anthony DURAND[a], Denis SORNIN[a*], Olivier TACHÉ[b], Thomas GUILBERT[a], François BRISSET[c], Ludovic DELBES[d], Benoît BAPTISTE[d], Thierry BAUDIN[c], Roland LOGÉ[e],

[a] Université Paris-Saclay, CEA, Service de Recherches Métallurgiques Appliquées, 91191, Gif-sur-Yvette, France.

[b] Université Paris-Saclay, CEA, CNRS, LIONS, NIMBE, 91191, Gif-sur-Yvette, France.

[c] Université Paris-Saclay, CNRS, Institut de chimie moléculaire et des matériaux d'Orsay, 91405, Orsay, France.

[d] Sorbonne Université, UMR CNRS 7590, Institut de Minéralogie, de Physique des Matériaux et de Cosmochimie, 75005, Paris, France.

[e] EPFL, Material institute, LMTM. MCA1 258 (Bât. Microcity), rue de la Maladiére 71b-CP526, CH-2002 Neuchâtel, Switzerland.

* Corresponding author: denis.sornin@cea.fr

## ABSTRACT

The development of generation IV nuclear reactor requires improvements in structural and cladding materials. Oxide dispersion strengthened (ODS) steels are promising candidates because of improved creep properties. Two main families of ODS steels are known, the first one is martensitic ODS steel with a full reverse ferrite to austenite phase transformation at high temperatures. The second one is ferritic ODS steels with a ferritic matrix whatever is the temperature. Previous papers mention the existence of untransformed ferrite (UF) phase at high temperature in very particular martensitic ODS steels [S. Ukai 2009, M. Yamamoto 2010, T. Yamashiro 2016, A. Durand 2021]. UF is unexpected according to experimental observation and thermodynamic calculations of the non-strengthened materials (NR) with same chemical composition. This UF is particularly interesting because UF is a way to improve the creep resistance of martensitic grades [H. Sakasegawa 2008, A. Durand 2021] and then conciliates the benefits of both ferritic and martensitic grades. The present study is focused on the thermal stability of untransformed ferrite (UF) in a martensitic ODS steel at 10 wt% Cr. Effects of the heat treatments holding times and temperatures are studied by considering the UF fraction evolution and microstructural changes. The decrease of UF fraction is correlated with the decrease of the nano-oxides density coupled to the increase of their size. The phase transformation temperatures of ODS steels are also affected by heat treatments. Those temperatures appear as a mix of the ODS and the equivalent non-strengthened materials ones.

Keywords: Untransformed Ferrite (UF), ODS steel, ferrito-martensitic steels, microstructure, SAXS.

## 1. INTRODUCTION

The development of the future generation of nuclear power plants (generation IV or fusion reactors) requires improvements in structural and cladding materials, particularly in terms of thermal creep. In fact, the working temperature increases from around 350°C for the generation II or III to around 650°C for generation IV. Considering void swelling, face-centered cubic (fcc) materials like austenitic steels cannot be safely employed beyond a neutron irradiation of 100 dpa [1]. Martensitic or ferritic steels, body-centered cubic (bcc) materials, are preferred considering the resistance to neutron irradiation. Nonetheless, the creep properties of those steels are worse than austenitic steels [2]. A considered solution is to improve the creep properties of bcc materials by adding nano-oxides. There are oxide dispersion strengthened (ODS) materials. They could combine the resistance to neutron irradiation of bcc materials and a sufficient creep resistance by the matrix strengthening [3,4]. In that view, ODS steels are prospect in the world [5,6]. Particular ODS steel grades, the martensitic ODS steels exhibit a phase transformation $\alpha \rightarrow \gamma$ (ferrite to

austenite) at high temperature. This phase transformation makes easier the cold manufacturing [7,8] and gives relatively isotropic mechanical properties [9]. On the contrary, ferritic ODS steels present always a ferritic phase. Then, there is no $\alpha \to \gamma$ phase transformation to facilitate the cold forming thanks to recovery heat treatments. However, those ferritic ODS steels remain very serious candidate for generation IV because of their better creep resistance than martensitic ODS steel [10]. To conciliate the benefits of ferritic ODS in term of creep resistance and martensitic ODS in the view of cold rolling, a new type of martensitic grades is highlighted for a few years. This is the martensitic ODS steel with untransformed ferrite (or residual ferrite) [11–14]. This consists in an ODS martensitic steel with a portion of material that does not change phase at high temperature. This untransformed ferrite (UF) seems to improve the creep resistance of martensitic grades [15,11,16]. Considering the non-strengthened base material chemical composition, thermodynamic calculations do not predict UF [13,14]. Those calculations are in agreement with observations in non-strengthened materials (NR) materials consolidated from metal powder without milling and $Y_2O_3$ addition [17]. Therefore, it appears that ODS reinforcement could considerably modify the reverse $\alpha$ to $\gamma$ phase transformation until leading to the untransformed phase [18]. However, the thermal stability of this UF is only documented in few papers [19], and appears as a crucial issue. Indeed, microstructural evolutions, including UF, of such grades in service and accidental conditions could be detrimental to the nuclear safety.

The main purpose of this study is to show, the effects of the temperature and duration of heat treatments on the UF fraction into a martensitic ODS steel, elaborated at the CEA and containing about 50% of UF [14]. Those results are discussed regarding the nano-oxides distribution and microstructures.

## 2. MATERIALS AND EXPERIMENTS

The material studied here is a 10 wt% Cr steel reinforced by nano-oxides, named 10Cr ODS thereafter. This ODS steel is elaborated following a powder metallurgy route. The pre-alloyed powder (about 2 Kg) is mechanically alloyed in a high-energy attritor with 0.1 wt% of $TiH_2$ powder and 0.3 wt% of $Y_2O_3$ powder under a helium atmosphere. The milled powder is hot extruded at 1050°C with an extrusion ratio of 9.8. More details of the chemical composition and elaboration process are available in a previous study [14].

A 10 wt% Cr steel without reinforcement by nano-oxides (NR) and free from untransformed ferrite, noted 10Cr, is also used as a reference. 10Cr material is obtained from the same powder as 10Cr ODS but not milled and without addition of $TiH_2$ and $Y_2O_3$. The powder is hot extruded in the exact same conditions as 10Cr ODS.

To evidence phases in samples (particularly UF), X-ray diffraction (XRD) at low and high temperatures is conducted on Panalytical Xper't Pro MPD diffractometer equipped with a cobalt X-ray sealed tube ($\lambda_{Co-K\alpha_1} = 1.78901$ Å and $\lambda_{Co-K\alpha_2} = 1.79290$ Å) and a XCelerator detector. $K\alpha_1$ and $K\alpha_2$ are very close leading to a double peak on the XRD measurements when Bragg conditions are reached. Bulk-material samples are studied in a controlled-atmosphere furnace from Anton Paar (HTK 1200N high temperature chamber). To avoid the grain morphology anisotropy, the analyzed surface is transverse to the extrusion direction. The furnace chamber is maintained under vacuum ($10^{-3}$ mBar) to prevent an excessive oxidation. The ferrite phase is body-centered cubic (bcc) and the austenite is face-centered cubic (fcc). According to the Bragg's law, the two phases present their diffraction peaks at different angular positions. Here, the prospected angle extent is [48°, 56°] including the (111) austenite at $2\theta = 50.2°$ ($d_{111} = 2.11$ Å) and (110) ferrite at $2\theta = 52.2°$ ($d_{110} = 2.04$ Å) diffraction peaks.

Differential scanning calorimetry (DSC), using a high temperature and sensitivity SETARAM MHTC96 equipment, allows us to measure phase transformation specific enthalpy ($\Delta H_{Ac_1 - Ac_3}$). $Ac_1$ and $Ac_3$ are, respectively, the beginning and the end of the $\alpha \rightarrow \gamma$ phase transformation. Samples are under high purity argon flow during the experiment. Samples are get from the consolidated material. Sample mass is around 4 g.

The observations in scanning electron microscopy are performed using the electron backscatter diffraction (EBSD). OIM software from EDAX is used to plot and analyze the maps. The surface was mechanically polished using diamond paste. A silica polishing is used to complete the preparation in the aim to release the surface stress.

The size and distribution of the nano-oxides are obtained from small angle X-ray scattering (SAXS) measurements in transmission mode. In this study, the sample thickness is grinded down to 75 μm in order to achieve a suitable transmission regarding the energy used. Experiments were performed at the CEA NIMBE/LIONS [20]. The energy of the X-ray beam is 17.4 keV ($\lambda = 0.704455$ Å). The nano-oxides are assumed mainly $Y_2Ti_2O_7$ pyrochlores [11,21]. The value of the electronic contrast, between the matrix Fe(bal.)-10Cr-1W (wt%) and the nano-oxides, is get thanks to tabulated data from Henke et al. study [22]. The analysis of the obtained scattering curve is performed using a Monte Carlo algorithm, McSAS [23,24]. The output data are the radius number distribution and the radius volume fraction distribution of the scattered particles. From those outputs, the mean radius (volume and number) and the number density of precipitates are estimated.

The purpose of this study is the stability of untransformed ferrite, in that view, different samples obtained from the 10Cr ODS are characterized. The first one, named **HE** is the material issued from the hot extrusion. **HT1** is the same material after a 1h-1050°C heat treatment under primary vacuum and cooled in the furnace at low speed 2°C/min. **HT10** corresponds to the HE material after a ten hours holding time at 1050°C heat treatment. The sample named **HTDSC** is the HE material submitted to a specific heat treatment into the DSC. The details of this heat treatment are presented in figure 1. Three different heats are performed in the aim to follow the variations of the heat flow after the previous heat and then measure the phase transformation specific enthalpy. The three heat cycles are done at a rate of 10°C/min and the cooling rate is set at −20°C/min after the targeted temperature is reached for 60s.



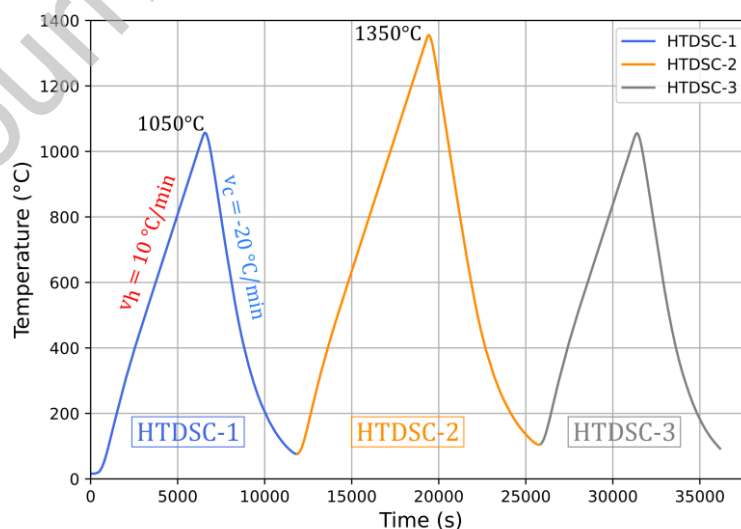Figure 1 : Heat treatments of HTDSC sample. The first cycle in blue is **HTDSC-1** (1050°C), the second in orange is **HTDSC-2** (1350°C) and the third in grey is **HTDSC-3** (1050°C).

Only the target temperature is different. The first one is a 1050°C heat treatment (**HTDSC-1**), the second is a 1350°C heat treatment (**HTDSC-2**) and the third is again at 1050°C (**HTDSC-3**). The effect of the 1350°C

heat treatment is then observed in the third cycle. **HTDSC** represents the material after these three heat steps into the DSC.

# 3. RESULTS

## 3.1. HEAT TREATMENT HOLDING TIME EFFECT

Previous study [14], illustrated the presence of UF at 1050°C which is the temperature of the powder consolidation. The figure 2 (a), according to [14], recaps the XRD measurements of the **HT1** sample at this temperature of 1050°C (red curve). This figure presents also a XRD measurement after twenty minutes of dwell time at 1050°C (orange curve). At room temperature (before heating and after cooling), only one peak is observed, the one of ferrite. At 1050°C, coexistence of austenite and ferrite is noted, even after twenty minutes of dwell time. The peak of ferrite detected at 1050°C is the UF peak. This UF peak is still present after twenty minutes which is in favour of a good stability of UF at this temperature. The 2θ position of ferrite peak displacement between room temperature and 1050°C is due to the thermal expansion of the crystal structure.
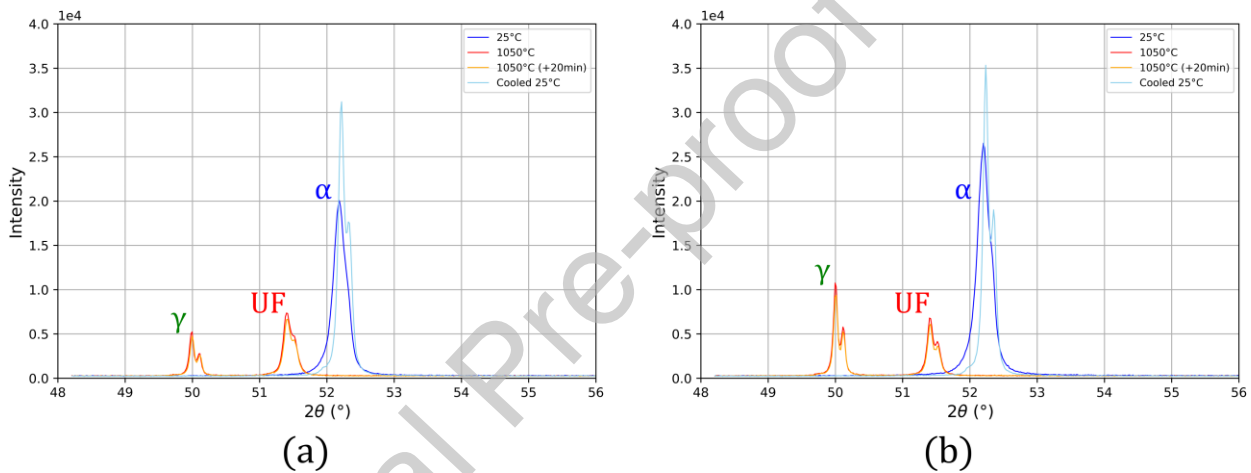


Figure 2 : XRD at 25°C before heat (darkblue), at 1050°C (red), at 1050°C and twenty minutes of holding time (orange) and 25°C after cooling (light blue) for (a) **HT1** and (b) **HT10** samples. Fig.2 (a) is issued from [14].

A longer heat treatment (many hours) into the XRD chamber is not prospected because of an excessive risk of sample oxidation in spite of the vacuum in the chamber. It is the reason why longer heat treatments are performed before XRD measurements. The **HT10** material is also studied by XRD. Results are presented in the figure 2 (b). After an *ex situ* heat treatment at 1050°C for ten hours and an *in situ* one for twenty minutes, UF peak is observed. Then, UF seems to be stabled at 1050°C. Nevertheless, the peak intensity ratio between the one of austenite and ferrite appears to change comparing **HT1** and **HT10**, traducing, probably, an evolution of the UF fraction after this heat treatment of ten hours. Unfortunately, experimental conditions do not allow a quantification of phases fractions in XRD at 1050°C. A too long holding time at 1050°C is required to acquire the entire angle extent necessary to conduct a Rietveld refinement giving the phases fractions.

If XRD measurements conclude to UF stability even after ten hours at 1050°C, the UF fraction determination is needed to complete this analysis. Two protocols are used to get this fraction, the first one is a dilatometric protocol (detailed in the previous work [14]) and the second one is based on the specific enthalpy measurement in DSC. The UF volume fraction by DSC method is get from the measurement of the phase transformation specific enthalpy. 10Cr ODS material presents an incomplete phase transformation, in comparison with the reference 10Cr, because of the presence of UF. 10Cr is fully austenitic at 1050°C

4

according to XRD measurements showed in figure 3. The phase transformation specific enthalpy is in agreement with values get from similar grades with a full transformation [25]. The presence of UF is evidenced in DSC by a weaker specific enthalpy of phase transformation as presented in table 1. Indeed, the amount of material that changes phases in 10Cr ODS is lower than in 10Cr.

Table 1 : Measured specific enthalpy during the α→γ transformation with a heating rate of 10°C/min for 10Cr and 10Cr ODS materials (CEA reference Q12) after hot extrusion.

| | $\Delta H$ (J/g) | State |
|---|---|---|
| 10Cr | $10.7 \pm 0.5$ | Full transformed |
| 10Cr ODS | $5.1 \pm 0.5$ | Untransformed ferrite |
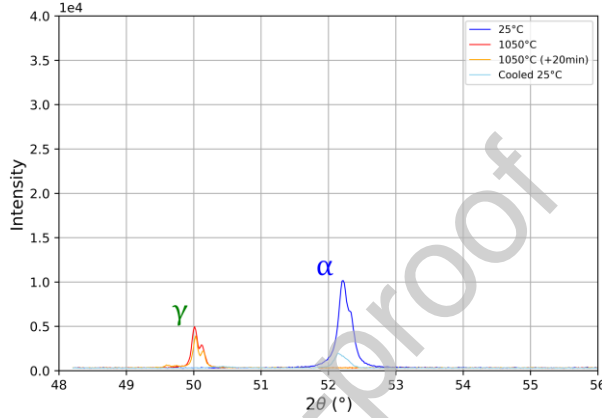


Figure 3 : XRD at 25°C before heat (darkblue), at 1050°C (red), at 1050°C and twenty minutes of keeping (orange) and 25°C after cooling (light blue) for 10Cr material (non ODS).

To estimate the volume fraction of material that does not change phase the specific enthalpy of the phase transformation of 10Cr ODS is compared to 10Cr assumed as a reference. Not only 10Cr presents a full phase transformation but also has a chemical composition close to 10Cr ODS. It is considered that the main part of Y and $TiH_2$ added in 10Cr ODS is contained into the nano-oxides and not in solution into the matrix. Finally, by adjusting the equation proposed by Dadé et al. [25], the estimation of the untransformed ferrite is :

$$\Delta H^{10Cr\ ODS}_{Ac_1-Ac_3} = (1-x) * \Delta H^{10Cr}_{Ac_1-Ac_3} \quad (1)$$

Where $x$ is the fraction of untransformed ferrite, $\Delta H^{10Cr\ ODS}_{Ac_1-Ac_3}$ and $\Delta H^{10Cr}_{Ac_1-Ac_3}$ are the phase transformation specific enthalpy of the 10Cr ODS and 10Cr respectively.

The UF volume fractions obtained by the two methods are summarized in the table 2.

Table 2 : UF volume fractions of **HE** an **HT10** obtained by dilatometric method and DSC method.

| | UF volume fraction (%) | |
|---|---|---|
| | Dilatometry | DSC |
| HE | $43.6 \pm 1.1$ | 52.7 |
| HT10 | $41.0 \pm 2.0$ | 39.4 |

The 1050°C heat treatment affects moderately the UF fraction into the 10Cr ODS material, despite ten hours of heat treatment.

## 3.2. HEAT TREATMENT TEMPERATURE EFFECT

To evidence the effect of the temperature on the UF, a particular heat treatment is conduct into the DSC (figure 1). The peak temperature studied here is 1350°C. The DSC methodology offers the opportunity to easily obtain, during the heat treatment, the UF fraction by measuring the specific enthalpy of the phase transformation (§3.1.). **HTDSC-1** is the first heating of 10Cr ODS after the hot extrusion and considered as a reference. **HTDSC-2** constitutes the heat treatment at 1350°C. **HTDSC-3** gives the consequence of this heat treatment measuring a third time the specific enthalpy of the α→γ transformation. The evolution of the heat flow during this heat procedure is illustrated in figure 4.
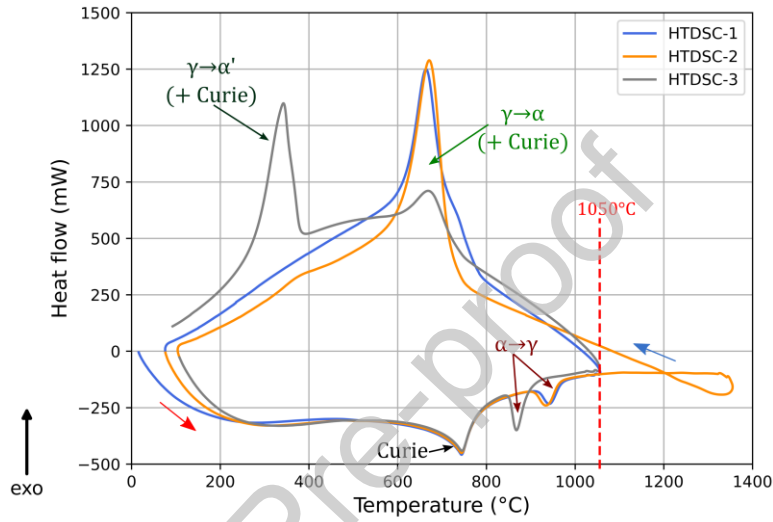


Figure 4 : Heat flow of the 10Cr ODS sample during the DSC heat treatment composed of three different heats (figure 1).

The values of the specific enthalpy and the UF fraction are detailed in table 3.

Table 3 : Phase transformation temperatures, measured specific enthalpy during the α→γ transformation with a heating rate of 10°C/min and UF volume fraction of **HTDSC-1-2-3**.

| | $Ac_1$ (°C) | $Ac_3$ (°C) | $\Delta H_{Ac_1-Ac_3}^{HTDSC-x}$ (J/g) | UF volume fraction (%) $1 - \dfrac{\Delta H_{Ac_1-Ac_3}^{HTDSC-x}}{\Delta H_{Ac_1-Ac_3}^{10Cr}}$ |
|---|---|---|---|---|
| HTDSC-1 | 916.4 | 968.5 | 4.5 | 58.2 |
| HTDSC-2 | 906.8 | 963.5 | 5.4 | 49.4 |
| HTDSC-3 | 851.9 | 894.2 | 8.0 | 25.0 |

After the first heat treatment, the UF fraction is slightly dwindled from 58.2% to 49.4%, consistently with an increase of the specific enthalpy. This is in agreement with the §3.1. where the 1050°C heat treatment was suspected to reduce a bit the UF fraction. In contrast, after 1350°C heat treatment, by comparing **HTDSC-1** and **HTDSC-3**, the UF fraction is reduced by half. Moreover, the phase transformation temperatures are significantly reduced, about 65°C for $Ac_1$ and 75°C for $Ac_3$. It can be noticed that, for the cooling of the last treatment **HTDSC-3**, a partial martensitic transformation occurs whereas the cooling rate does not change (grey curve in figure 4).

The 1350°C heat treatment affects much more the UF fraction than the ones at 1050°C.

6

## 3.3. Nano-particles and microstructure evolutions

### 3.3.1. SAXS measurements

The figure 5 presents the scattering curves obtained by SAXS measurements of the four samples **HE**, **HT1**, **HT10** and **HTDSC**. The inflection of the scattering curves (noted by arrows) represents the q-position of the main particle contribution on the scattering curve. An inflexion at a lower q-position indicates a contribution of larger particles [26,27]. Consequently, **HTDSC** appears to have the largest particles and **HE** the smallest. Thus, the shape of scattering curves illustrates the scattering of very different particle size for **HTDSC** compared to **HE**, **HT1** and **HT10** which are samples heat treated at lower temperature.
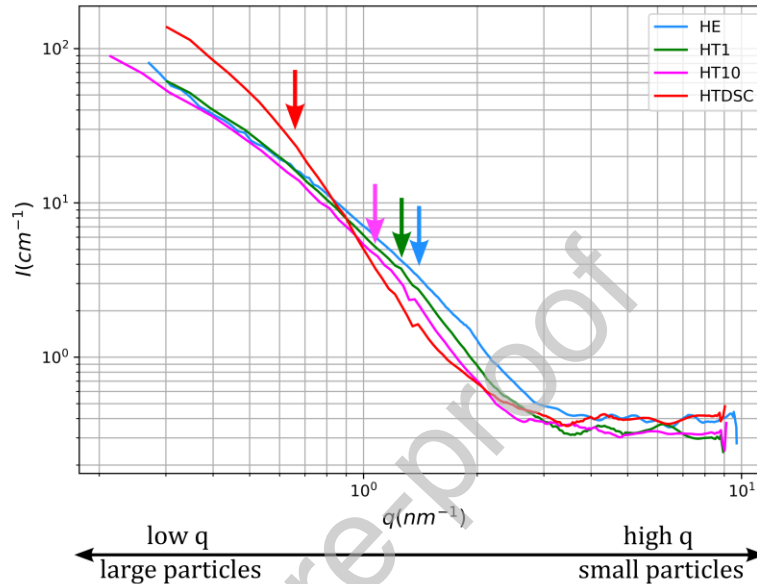


Figure 5 : Scattering curves of HE, HT1, HT10 and HTDSC samples. Arrows indicate the q-position of the main particles contribution on scattering.

The table 4 presents the average particles size and the density of particles calculated from the Monte Carlo method. The scattering curves observations are confirmed by those statistics. Indeed, **HTDSC** presents the largest particles and thus the smallest particles density.

Table 4 : Volume mean radius ($r_{vol}$), number mean radius ($r_{nb}$) and particles density (N) of **HE**, **HT1**, **HT10** and **HTDSC** measured by SAXS.

|  | $r_{vol}$ (nm) | $r_{nb}$ (nm) | $N \left( . 10^{23} \ m^{-3} \right)$ |
|---|---|---|---|
| HE | 2.58 | 1.02 | 4.56 |
| HT1 | 2.76 | 1.10 | 3.57 |
| HT10 | 2.99 | 1.14 | 2.93 |
| HTDSC | 4.52 | 1.28 | 1.23 |

### 3.3.2. EBSD observations

This section prospects the material microstructures, highlighting the UF phase evolutions after various heat treatments. The UF areas into the microstructure are identified by the distinction of ferrite (UF) phase and martensite phase into a quenched sample from 1050°C. Quench transforms the austenite at 1050°C into martensite whereas UF at 1050°C remains ferrite at low temperature. Based on EBSD indicator named

7

image quality (IQ), the distinction of the UF from the rest of the material is made possible at room temperature. An IQ threshold is conducted to separate the martensite from the ferrite [14]. The IQ value of the ferritic grains is greater than the one of the martensitic grains due to lower geometrically necessary dislocations. By plotting the grain inventory as function of the average IQ parameter of each grain, it appears a double peak curve. The threshold is arbitrarily fixed at the inflection point between the both peaks. To observe the UF in the microstructure, **HE**, **HT10** and **HTDSC** are quenched and observed in EBSD. The figure 6 presents the inverse pole figure maps (< uvw > direction parallel to the extrusion direction) and the IQ threshold maps (UF is plot in blue and martensite is in red).
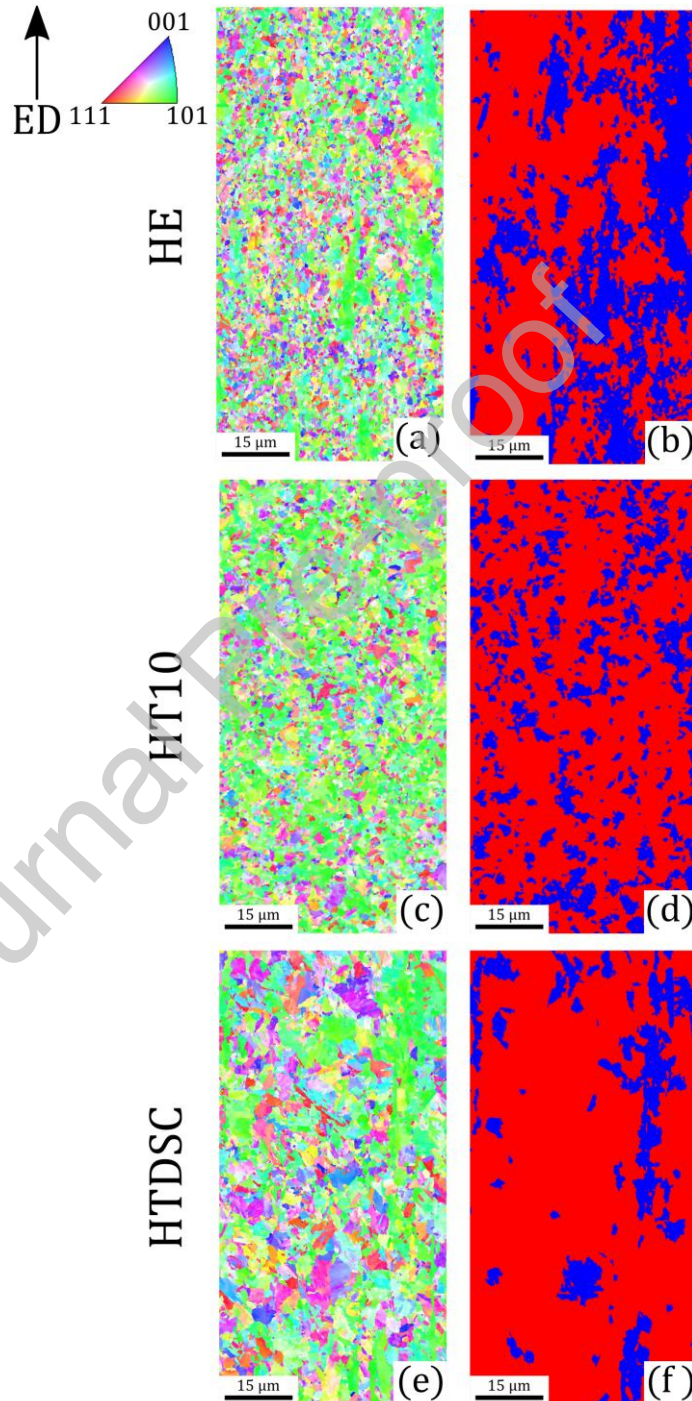


Figure 6 : Inverse pole figure map <uvw> direction parallel to the extrusion direction ED of (a) **HE** quenched, (c) **HT10** quenched and (e) **HTDSC** quenched. IQ threshold map of (b) **HE** quenched, (d) **HT10** quenched and (f) **HTDSC** quenched, martensite area are in red and UF area are in blue.

8

The UF areas are significantly reduced after the 1350°C heat treatment, only a few of small UF areas are still observed. Using the maps of Figure 6 the respective surfaces of UF (in blue) and martensite (in red) can be determined. Table 5 summarizes the surface fraction of untransformed ferrite obtained by the EBSD analysis.

Table 5 : Surface fraction of untransformed ferrite in 10 Cr ODS as hot extruded (HE), after 10h at 1050°C (HT10) and after 1350°C heat treatment (HTDSC). Values are obtained from EBSD maps of figure 6.

|  | UF surface fraction (%) |
|---|---|
| HE | 36 |
| HT10 | 25 |
| HTDSC | 15 |

The UF surface fractions values are lower compared to other methods. Indeed, this method is a surface fraction whereas other methods are volume methods. Besides, the EBSD maps explore a small part of the materials, even if authors chose carefully a representative area of the whole material.

In accordance with dilatometric and DSC quantifications, the diminution of the UF fraction is observed in the microstructures. Then, heat treatments affecting the UF fraction logically influence the microstructure and the distribution of UF.

It can be noticed that the untransformed ferrite alpha fibre (<110> || ED), the preferred grain orientation, is preserved during heat treatments. Therefore, green areas on inverse pole figure maps correspond mostly to UF domains. This is a confirmation of this method consistency.

# 4. DISCUSSION

The results of §3. present the contribution of the heat treatment holding time and temperature effects on the UF stability. Oka et al. [19] have already documented evolutions of the UF fraction under various thermo-mechanical treatments of a same (HIP) initial microstructure. Here, the present study results are discussed regarding, more specifically, the nano-oxides distribution and the associated microstructural evolutions.

The heat treatment dwell time at 1050°C affects moderately the UF fraction (§3.1.). The microstructure shows, after ten hours of treatment, smaller and more dispersed UF areas but UF is still present at high volume fraction. The EBSD analysis of the surface fraction of UF, highlights a much more important decrease of the UF surface fraction after the 1350°C heat treatment than after the 10 hours heat treatment at 1050°C. Considering the nano-oxides, heat treatments at 1050°C let grow weakly the oxides (§3.3.1.). On the contrary, 1350°C heat treatment leads to a drop of UF fraction (§3.2.). This reduction is associated to a very different microstructure and a large coarsening of the nano-oxides compared to the reference **HE**. This last tendency is consistent with previous studies like [28]. These results show a correlation between the drop of UF fraction and the nano-oxides growth (and thus the decrease of the particles density). This correlation is evidenced by the figure 7. A decrease in UF fraction is linked to a decrease of the nano-oxides density. Contrarily to previous works of Ohtsuka *et al*, this observation is made for various precipitation distributions of a single grade (10Cr) without significant chemical composition change [18]. Previous studies show that nano-oxides are smaller in the UF ferrite than in the martensite (the part of the material that changes phase) [11,29,30]. Considering those studies, the increase of nano-oxides size is in agreement with the decrease of the UF fraction. Nonetheless, the particles growth observed here is not very significant during the heat treatment at 1050°C although this temperature is more than 100°C above the phase

transformation temperature $Ac_3$ (see figure 4, phase transformation temperatures of the **HTDSC-1** treatment). This last finding is consistent with the nano-oxides thermal stability threshold documented around 1150°C [31]. The work of Kim *et al.* [32] illustrates two domains of particles growth in a 9Cr ODS steel which are in agreement with the two temperature domains of the present study (1050°C and 1350°C). Unexpectedly, after 1050°C 10 hours, a duration not currently depicted in previous papers, nano-precipitates density is affected. Consequently, we must conclude that, for our material, the stability threshold discussed above is reached at lower temperature than 1050°C. Here it is not possible to know if the UF fraction drops because of the precipitates coarsening or inversely. The cause/effect relationship between the nano-oxides size growth and the UF fraction drop is still a main question.
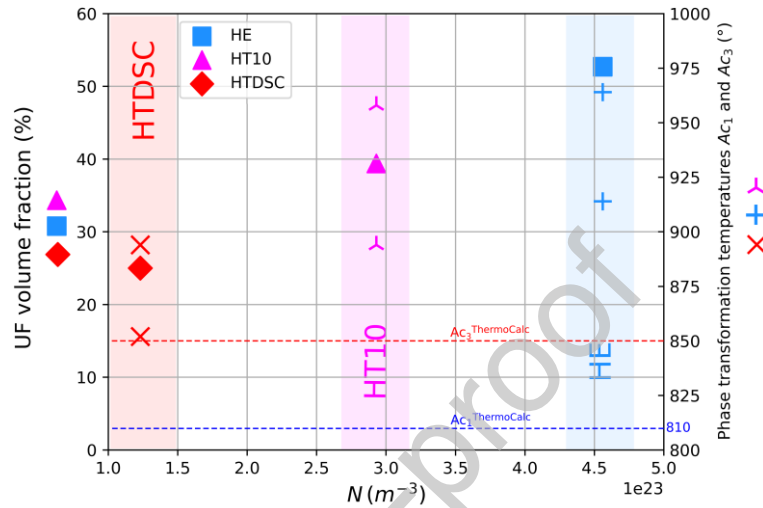


Figure 7 : UF volume fraction measured by DSC and phase transformation temperatures $Ac_1$, $Ac_3$ measured by DSC with a heating rate of 10°C/min as a function of the nano-oxides density obtained by SAXS with Monte Carlo method. The dot lines represent $Ac_1$ and $Ac_3$ obtained from ThermoCalc calculations for to the 10Cr materials of the study without the oxide dispersion contribution [14].

The microstructure (grain size and UF areas) changes a lot after 1350°C, the grain size increases and the UF areas decreases. The grain growth observed on the quenched sample (figure 6-e) may proceed from austenitic grain growth. This assumption is consistent with the martensitic transformation which occurs during the cooling of **HTDSC-3**. The austenitic grain size growth promotes the reduction of the critical cooling rate for martensitic transformation. Beside, ODS steels present very high critical cooling rate because of very small prior austenite grains [33].

According to those results, it can be concluded that there is a correlation between the nano-oxides growth and the microstructural changes, including the UF areas fraction. The variations of UF areas and fraction are concurrent to modifications of phase transformation temperatures $Ac_1$ and $Ac_3$ as summed up by figure 7. Previous study [14] presents a thermodynamic computation of a grade with the same chemical composition as the present ODS grade but without reinforcement consideration. These computed phase transformation temperatures are indicated on figures 7 (dot lines). Phase transformation temperatures are known to be higher for ODS steels [34]. Moreover, the phase transformation specific enthalpy of the 10Cr ODS steel after 1350°C heat treatment (HTDSC-3 in table 3) increases compared to the initial HE material. (table 1). Then, the decrease of $Ac_1$ and $Ac_3$ and the increase of the specific enthalpy observed after the 1350°C heat treatment appear as an intermediate behaviour between the initial ODS steel and the equivalent non-strengthened material. Consequently, it can be concluded that, like the UF fraction, phase transformation temperatures and enthalpy are directly related to the nano-precipitation density.

10

# CONCLUSION

Previous papers mention the existence of untransformed ferrite (UF) phase at high temperature in ODS steels [11–14]. UF contributes to the creep resistance improvement of martensitic grades [15,11] and then conciliate the benefits of the ferritic and martensitic grades. However, the thermal stability of such UF was not extensively prospected. The present study is focused on the thermal stability of UF in a martensitic ODS steel containing 10 wt% Cr.

The following conclusions are outline:

- 10Cr ODS containing untransformed ferrite phase exhibits a low decrease of the UF fraction after 1050°C heat treatments which correspond to the hot extrusion temperature. Even after ten hours at 1050°C, UF is still present with a slightly decreased volume fraction. After this treatment, the UF volume fraction of the initial material after hot extrusion decreases from 43.6% to 41% and 52.7% to 39.4%, respectively for dilatometry or DSC method.

- Ultra high temperature treatment at 1350°C affects a lot the nano-oxides size and the microstructure. The 1350°C heat treatment reduces by a half the UF fraction which is shown to be correlated to the nano-precipitates density reduction by 3.7 times. Heat treatments at temperatures exceeding hot extrusion one impact the UF fraction much more than long time heat treatments at temperature close to the hot extrusion one. This is consistent with the already documented thermal threshold for nano-precipitates coarsening.

- The 1050°C and the 1350°C heat treatments also affect the phase transformation temperatures $Ac_1$ and $Ac_3$. These characteristic temperatures and the UF fraction drop simultaneously. This drop is correlated with a reduction of nanoprecipitation density. The material heat treated at 1350°C exhibits intermediate phase transformation temperatures between the ones of the initial ODS material and an equivalent grade without reinforcement.

- After the 1350°C heat treatment, UF fraction decrease is concomitant to microstructure changes, including grain growth observed on the martensitic state, which is consistent with a reduced anchoring of grain boundaries by precipitates. Another consequence is a complete change of the critical cooling rate for martensitic transformation.

## CREDIT AUTHORSHIP CONTRIBUTION STATEMENT

**Anthony Durand:** Conceptualization, Methodology, Investigation, Data curation, Writing – original draft, Writing – review & editing. **Denis Sornin:** Conceptualization, Methodology, Investigation, Writing – original draft, Writing – review & editing. **Olivier Taché:** Investigation, Data curation, Validation, Formal analysis. **Thomas Guilbert:** Methodology, Investigation, Data curation, Writing – review & editing. **François Brisset:** Investigation, Validation, Data curation. **Ludovic Delbes:** Methodology, Investigation, Data curation, Writing – review & editing**. Benoît Baptiste:** Methodology, Investigation, Data curation, Validation, Writing – review & editing. **Thierry Baudin:** Conceptualization, Methodology, Writing – review & editing, Supervision. **Roland Logé:** Conceptualization, Methodology, Writing – review & editing, Supervision.

### Declaration of interests

The authors declare that they have no known competing financial interests or personal relationships that could have appeared to influence the work reported in this paper.

# ACKNOWLEDGEMENTS

# REFENRENCES

[1] P. Yvon, M. Le Flem, C. Cabet, J.L. Seran, Structural materials for next generation nuclear systems: Challenges and the path forward, Nucl. Eng. Des. 294 (2015) 161–169. https://doi.org/10.1016/j.nucengdes.2015.09.015.

[2] A. Alamo, V. Lambard, X. Averty, M.H. Mathon, Assessment of ODS-14%Cr ferritic alloy for high temperature applications, J. Nucl. Mater. 329–333 (2004) 333–337. https://doi.org/10.1016/j.jnucmat.2004.05.004.

[3] S. Ukai, M. Fujiwara, Perspective of ODS alloys application in nuclear environments, J. Nucl. Mater. 307 (2002) 749–757.

[4] R.L. Klueh, J.P. Shingledecker, R.W. Swindeman, D.T. Hoelzer, Oxide dispersion-strengthened steels: A comparison of some commercial and experimental alloys, J. Nucl. Mater. 341 (2005) 103–114. https://doi.org/10.1016/j.jnucmat.2005.01.017.

[5] S. Ukai, T. Nishida, H. Okada, T. Okuda, M. Fujiwara, K. Asabe, Development of Oxide Dispersion Strengthened Ferritic Steels for FBR Core Application, (I): Improvement of Mechanical Properties by Recrystallization Processing, J. Nucl. Sci. Technol. 34 (1997) 256–263. https://doi.org/10.1080/18811248.1997.9733658.

[6] M.K. Miller, D.T. Hoelzer, E.A. Kenik, K.F. Russell, Nanometer scale precipitation in ferritic MA/ODS alloy MA957, J. Nucl. Mater. 329–333 (2004) 338–341. https://doi.org/10.1016/j.jnucmat.2004.04.085.

[7] L. Toualbi, C. Cayron, P. Olier, J. Malaplate, M. Praud, M.-H. Mathon, D. Bossu, E. Rouesne, A. Montani, R. Logé, Y. de Carlan, Assessment of a new fabrication route for Fe–9Cr–1W ODS cladding tubes, J. Nucl. Mater. 428 (2012) 47–53. https://doi.org/10.1016/j.jnucmat.2011.12.013.

[8] E. Vakhitova, D. Sornin, F. Barcelo, M. François, Texture evolution in Oxide Dispersion Strengthened (ODS) steel tubes during pilgering process, J. Nucl. Mater. 494 (2017) 20–28. https://doi.org/10.1016/j.jnucmat.2017.07.002.

[9] T. Jaumier, S. Vincent, L. Vincent, R. Desmorat, Creep and damage anisotropies of 9%Cr and 14%Cr ODS steel cladding, J. Nucl. Mater. 518 (2019) 274–286. https://doi.org/10.1016/j.jnucmat.2019.02.041.

[10] J.-J. Huet, L. Coheur, A.D. Bremaecker, L.D. Wilde, J. Gedopt, W. Hendrix, W. Vandermeulen, Fabrication and Mechanical Properties of Oxide Dispersion Strengthening Ferritic Alloy Canning Tubes for Fast Reactor Fuel Pins, Nucl. Technol. 70 (1985) 215–219. https://doi.org/10.13182/NT85-A33645.

[11] S. Ukai, S. Ohtsuka, T. Kaito, H. Sakasegawa, N. Chikata, S. Hayashi, S. Ohnuki, High-temperature strength characterization of advanced 9Cr-ODS ferritic steels, Mater. Sci. Eng. A. 510–511 (2009) 115–120. https://doi.org/10.1016/j.msea.2008.04.126.

[12] M. Yamamoto, S. Ukai, S. Hayashi, T. Kaito, S. Ohtsuka, Reverse phase transformation from α to γ in 9Cr-ODS ferritic steels, J. Nucl. Mater. 417 (2011) 237–240. https://doi.org/10.1016/j.jnucmat.2010.12.250.

[13] T. Yamashiro, S. Ukai, N. Oono, S. Ohtsuka, T. Kaito, Microstructural stability of 11Cr ODS steel, J. Nucl. Mater. 472 (2016) 247–251. https://doi.org/10.1016/j.jnucmat.2016.01.002.

[14] A. Durand, D. Sornin, Y. de Carlan, G. Spartacus, F. Brisset, L. Delbes, B. Baptiste, T. Baudin, R. Logé, Characterization of untransformed ferrite in 10Cr and 12Cr ODS steels, Materialia. (2021) 101066. https://doi.org/10.1016/j.mtla.2021.101066.

[15] H. Sakasegawa, S. Ukai, M. Tamura, S. Ohtsuka, H. Tanigawa, H. Ogiwara, A. Kohyama, M. Fujiwara, Creep constitutive equation of dual phase 9Cr-ODS steel, J. Nucl. Mater. 373 (2008) 82–89. https://doi.org/10.1016/j.jnucmat.2007.05.031.

[16] H. Oka, T. Tanno, Y. Yano, S. Ohtsuka, T. Kaito, N. Hashimoto, Effect of nitrogen concentration on creep strength and microstructure of 9Cr-ODS ferritic/martensitic steel, J. Nucl. Mater. 572 (2022) 154032. https://doi.org/10.1016/j.jnucmat.2022.154032.

[17] S. Ukai, N. Oono-Hori, S. Ohtsuka, Oxide Dispersion Strengthened Steels, in: Compr. Nucl. Mater., Elsevier, 2020: pp. 255–292. https://doi.org/10.1016/B978-0-12-803581-8.11718-7.

[18]    S. Ohtsuka, T. Kaito, S. Kim, M. Inoue, T. Asayama, M. Ohnuma, J. Suzuki, Effect of Nano-Size Oxide Particle Dispersion and &delta;-Ferrite Proportion on Creep Strength of 9Cr-ODS Steel, Mater. Trans. 50 (2009) 1778–1784. https://doi.org/10.2320/matertrans.M2009096.

[19]    H. Oka, T. Tanno, S. Ohtsuka, Y. Yano, T. Uwaba, T. Kaito, M. Ohnuma, Effect of thermo-mechanical treatments on nano-structure of 9Cr-ODS steel, Nucl. Mater. Energy. 9 (2016) 346–352. https://doi.org/10.1016/j.nme.2016.10.007.

[20]    O. Taché, S. Rouzière, P. Joly, M. Amara, B. Fleury, A. Thill, P. Launois, O. Spalla, B. Abécassis, MOMAC: a SAXS/WAXS laboratory instrument dedicated to nanomaterials, J. Appl. Crystallogr. 49 (2016) 1624–1631. https://doi.org/10.1107/S1600576716012127.

[21]    G. Spartacus, J. Malaplate, F. De Geuser, D. Sornin, A. Gangloff, R. Guillou, A. Deschamps, Nano-oxide precipitation kinetics during the consolidation process of a ferritic oxide dispersion strengthened steel., Scr. Mater. 188 (2020) 10–15. https://doi.org/10.1016/j.scriptamat.2020.07.003.

[22]    B.L. Henke, E.M. Gullikson, J.C. Davis, X-Ray Interactions: Photoabsorption, Scattering, Transmission and Reflection, At. Data Nucl. Data Tables. 54 (1993) 1–170.

[23]    B.R. Pauw, J.S. Pedersen, S. Tardif, M. Takata, B.B. Iversen, Improvements and considerations for size distribution retrieval from small-angle scattering data by Monte Carlo methods, J. Appl. Crystallogr. 46 (2013) 365–371. https://doi.org/10.1107/S0021889813001295.

[24]    I. Bressler, B.R. Pauw, A.F. Thünemann, McSAS: software for the retrieval of model parameter distributions from scattering patterns, J. Appl. Crystallogr. 48 (2015) 962–969. https://doi.org/10.1107/S1600576715007347.

[25]    M. Dadé, J. Malaplate, J.C. Brachet, T. Guilbert, C. Toffolon-Masclet, Influence of chemical composition on the microstructure and phase transformations of Fe-14Cr ferritic steels, Materialia. 7 (2019) 100388. https://doi.org/10.1016/j.mtla.2019.100388.

[26]    T. Tanno, S. Ohtsuka, Y. Yano, T. Kaito, Y. Oba, M. Ohnuma, S. Koyama, K. Tanaka, Evaluation of mechanical properties and nano-meso structures of 9–11%Cr ODS steels, J. Nucl. Mater. 440 (2013) 568–574. https://doi.org/10.1016/j.jnucmat.2013.04.006.

[27]    H. Schnablegger, Y. Singh, The SAXS Guide, 3rd ed., 2017.

[28]    N. Oono, K. Nakamura, S. Ukai, T. Kaito, T. Torimaru, A. Kimura, S. Hayashi, Oxide particle coarsening at temperature over 1473 K in 9CrODS steel, Nucl. Mater. Energy. 9 (2016) 342–345. https://doi.org/10.1016/j.nme.2016.06.008.

[29]    M. Yamamoto, S. Ukai, S. Hayashi, T. Kaito, S. Ohtsuka, Formation of residual ferrite in 9Cr-ODS ferritic steels, Mater. Sci. Eng. A. 527 (2010) 4418–4423. https://doi.org/10.1016/j.msea.2010.03.079.

[30]    S. Ohtsuka, S. Ukai, H. Sakasegawa, M. Fujiwara, T. Kaito, T. Narita, Nano-mesoscopic structural characterization of 9Cr-ODS martensitic steel for improving creep strength, J. Nucl. Mater. 367–370 (2007) 160–165. https://doi.org/10.1016/j.jnucmat.2007.03.004.

[31]    S. Kim, S. Ohtsuka, T. Kaito, S. Yamashita, M. Inoue, T. Asayama, T. Shobu, Formation of nano-size oxide particles and δ-ferrite at elevated temperature in 9Cr-ODS steel, J. Nucl. Mater. 417 (2011) 209–212. https://doi.org/10.1016/j.jnucmat.2011.01.063.

[32]    S.-W. Kim, T. Shobu, S. Ohtsuka, T. Kaito, M. Inoue, M. Ohnuma, Kinetic Approach for Growth and Coalescence of Nano-Size Oxide Particles in 9Cr-ODS Steel Using High-Energy Synchrotron Radiation X-rays in SPring-8, Mater. Trans. 50 (2009) 917–921. https://doi.org/10.2320/matertrans.MER2008439.

[33]    S. Ukai, S. Mizuta, M. Fujiwara, T. Okuda, T. Kobayashi, Development of 9Cr-ODS Martensitic Steel Claddings for Fuel Pins by means of Ferrite to Austenite Phase Transformation, J. Nucl. Sci. Technol. 39 (2002) 778–788. https://doi.org/10.1080/18811248.2002.9715260.

[34]    C. Cayron, E. Rath, I. Chu, S. Launois, Microstructural evolution of Y2O3 and MgAl2O4 ODS EUROFER steels during their elaboration by mechanical milling and hot isostatic pressing, J. Nucl. Mater. 335 (2004) 83–102. https://doi.org/10.1016/j.jnucmat.2004.06.010.

.